Available online at www.sciencedirect.com
ScienceDirect
Journal of Computational Physics 227 (2008) 5256–5271
JOURNAL OF COMPUTATIONAL PHYSICS
www.elsevier.com/locate/jcp

A discrete velocity direction model for the Boltzmann equation and applications to micro gas flows

Zhenyu Zhang [a,*], Jianzhong Xu [b], Zhiguo Qi [b], Guang Xi [a]

[a] School of Energy and Power Engineering, Xi'an Jiaotong University, Xi'an 710049, China
[b] Institute of Engineering Thermophysics, Chinese Academy of Sciences, Beijing 100080, China

Received 26 June 2007; received in revised form 22 January 2008; accepted 23 January 2008
Available online 2 February 2008

Abstract

A discrete velocity direction model for the Boltzmann equation is proposed in this paper, which provides an alternative technique to the rarefied gas flows. In this model, the directions of molecular velocities are discrete, which are restricted in eight fixed directions, while the molecular speed rate is still continuous. By this approximation, the Boltzmann equation in the six-dimensional phase space is replaced by eight differential-integral equations in three-dimensional space. Thus, the computational cost is reduced greatly by reduction of three dimensions. The number of discrete velocities is not fixed in the present model because the speed rate can be truncated arbitrarily. This is distinguished from the conventional discrete velocity models (DVM). To test this technique, it was applied to the Couette flow and Poiseuille flow. The computed results agree well with those by the linearized Boltzmann equation and the DSMC method.

Keywords: Discrete velocity direction model; Boltzmann equation; Low-speed; Micro flow

1. Introduction

The micro-electro-mechanical system (MEMS) has developed rapidly in recent years with the development of micro fabrication technology [1]. In the small systems, the characteristic lengths usually range from sub-millimeter to sub-micrometer and gas flows always enter the slip regime, even the transition regime [2,3]. The Knudsen number can range from 0.01 to 10 [4]. To understand this kind of flow, some fundamental experiments have been carried out [5–7]. These investigations disclosed that the behavior of micro flows differs greatly from that of the macro flows [2,8]. Phenomena in rarefied gas flows have been observed in micro gas flows, such as velocity-slip and temperature-jump. Due to the limitation of current experimental conditions, these experiments were mainly limited to some simple structures, such as micro channels and micro nozzles [3]. Thus, up to now, studies on the micro gas flows still mainly rely on theoretical and computational techniques.

* Corresponding author. Tel./fax: +86 029 82668783.
E-mail address: zhangzy78@gmail.com (Z. Zhang).

0021-9991/$ - see front matter © 2008 Elsevier Inc. All rights reserved.
doi:10.1016/j.jcp.2008.01.030

In rarefied gas flows, the continuous medium hypothesis and the Navier–Stokes equation with no-slip boundary condition are not valid any more [4,9]. The Boltzmann equation should be employed as the governing equation. It is a very complicated differential-integral equation and the integral term contains the products of unknown variables [9,10]. Up to now, analytical solutions are only for very simple flow conditions. For most flow conditions, Boltzmann equation still cannot be solved by analytical method. On the other hand, it is very difficult to be solved by the numerical methods directly [11]. The reason is that the Boltzmann equation is in the six-dimensional phase space and contains seven independent variables (x, y, z, c_x, c_y, c_z, t). The existence of many dimensions needs such a large number of points, thus the computational cost becoming very expensive. For example, even for the steady flow, the number of points will reach 10^6 if there are only 10 points in each dimension. To our knowledge, usually 10 points in each dimension are not enough in numerical calculations. So, up to now, this method cannot be widely used under current computational conditions [11].

To avoid the difficulty of the Boltzmann equation, some simulation methods were proposed, such as the Monte–Carlo methods. In these simulation methods, the direct simulation Monte–Carlo (DSMC) method is the most used method for rarefied gas flows [2–4,11,12]. But this method meets a great trouble in micro flows because of low-speed. In micro flows, most flows are subsonic and usually the macro velocities of flows are much lower than the thermal velocity at room temperature, such as the gas flows in MEMS [2]. It is very difficult to obtain statistically convergent results under the low-speed condition for DSMC method. To reduce the statistical scatter effectively, an extremely large sample size is required. Then the computational cost becomes very expensive. To overcome this difficulty, the information preservation (IP) method and a molecular block model DSMC method are proposed [2,12]. Besides the simulation methods, some methods by reducing the Boltzmann equation were also proposed, such as the Chapman–Enskog method, Grad 13 moment equations, BGK model equation, linearized Boltzmann equation, linearized model equation, transition probability matrix (TPM) method, convective scheme (CS) method, discrete velocity models (DVM) and so on [9–27], in which the linearized Boltzmann equation gives the most accurate solution. But this method is very computationally expensive [19].

To reduce the computational cost, a discrete velocity direction model is presented in this paper. In this model, the molecular velocity directions are fixed into eight discrete directions and the molecular speed rate is still continuous. In the conventional discrete velocity models, the molecular velocities are restricted into a finite set and the Boltzmann equation is reduced into a set of differential equations, in which the variables are number densities $n_i(\vec{r}, t)$, such as the models proposed by Broadwell, Cabannes and Gatignol [9,13,19,20,28–30]. But in the present model, only the velocity directions are discrete. By this approximation, the six-dimensional Boltzmann equation is reduced to a set of three-dimensional differential-integral equations and the integral terms still contain the products of unknown variables. Though these equations are still very difficult, the computational cost can be reduced greatly due to the six-dimensional velocity distribution function $f(\vec{r}, \vec{c}, t)$ is replaced by the three-dimensional speed distribution function $f_i(\vec{r}, t)$ like the DVM. But the number of discrete velocities is not fixed because the speed rate is continuous in the present model. The speed rate will be truncated further into a finite set in numerical calculations and the number of velocities depends on the computational condition. To test this model, the Couette flow and the Poiseuille flow in microscale were investigated. The Knudsen number ranges from 0.01 to 10. Because the low-speed flows are more interesting in micro flow, the characteristic velocities in the Couette flow and Poiseuille flow are much lower than the thermal velocity. The plate velocity is 0.1 m/s in Couette flow and the largest velocity is less than 0.1 m/s in Poiseuille flow. The velocity distributions, shearing stress and mass flux given by the present model compare well with the results by the linearized Boltzmann equation and the DSMC method when the Knudsen number is not large. But at large Knudsen number, the results given by the present model deviate clearly from the Boltzmann equation, which just like the discrete velocity models.

2. Discrete velocity direction model

2.1. Basic assumptions

In the model, molecular velocities are restricted in eight discrete directions, but the distribution of speed rate is still continuous. Eight discrete directions are defined as follows: establish a cube in a rectangular

coordinate system. Put its center at the origin and let its sides be vertical to the coordinate axes. Then these directions from the origin to eight apexes are the assumed directions. The sequence of eight directions is shown in Fig. 1. To be convenient, the molecules are the same hard spheres and no external force acts on them.

2.2. Definitions of the speed distribution functions

In the discrete velocity direction model, the variables are eight speed distribution functions. They are defined as $f_i(c_i, \vec{r}, t), (i = 1, 2, \ldots, 8)$, in which c_i $(0 \leqslant c_i < \infty)$ is the molecular speed rate in direction $i, \vec{r}$ is the position vector and t is the time variable. The meaning of these variables is that in the moment $t, c \in (c_i, c_i + \mathrm{d}c_i), \vec{r} \in (\vec{r}, \vec{r} + \mathrm{d}\vec{r})$, the number of molecules moving towards direction i is $f_i(c_i, \vec{r}, t)\,\mathrm{d}\vec{r}\,\mathrm{d}c_i$.

Consider a group of molecules in a finite volume $\mathrm{d}\vec{r}$, which speed rate is between c_i and $c_i + \mathrm{d}c_i$. Due to the impact effect, the molecular number will be $f_i(c_i, \vec{r} + c_i\vec{l}_i\mathrm{d}t, t + \mathrm{d}t)\mathrm{d}\vec{r}\mathrm{d}c_i$ during a time interval $\mathrm{d}t$, in which $\vec{l}_i$ is the unit vector in direction i. The change of the molecular number can be described by the following equation:

$$f_i(c_i, \vec{r} + c_i\vec{l}_i\,\mathrm{d}t, t + \mathrm{d}t)\,\mathrm{d}\vec{r}\,\mathrm{d}c_i - f_i(c_i, \vec{r}, t)\,\mathrm{d}\vec{r}\,\mathrm{d}c_i = (G_i - L_i)\,\mathrm{d}\vec{r}\,\mathrm{d}c_i\,\mathrm{d}t, \tag{1}$$

in which, G_i is the gaining term and L_i is the losing term. Divide Eq. (1) by the term $\mathrm{d}\vec{r}\,\mathrm{d}c_i\,\mathrm{d}t$ and let t approach zero. Then

$$\frac{\partial f_i}{\partial t} + c_i\vec{l}_i\frac{\partial f_i}{\partial \vec{r}} = G_i - L_i, \quad (i = 1, 2, \ldots, 8), \tag{2}$$

2.3. Molecular collision

In order to gain the expressions of these gaining terms and losing terms, the collision law in the present model should be studied first. Due to the characteristic of centrosymmetry of this model, the binary collisions can be classified into four kinds according to the impact angles. Four impact angles are $0, 2\mathrm{arctg}\sqrt{2}/2$, $2\mathrm{arctg}\sqrt{2}$ and π. The scattering way must obey the following rules: molecules still move in eight restricted directions and the total momentum and energy of each couple of molecules keep conservation after collision. Take the binary collisions with molecules in direction 1 for instance.

(1) Included angles are equal to 0. In this binary collision, two molecules will change their velocities and still move in this direction after collision. To be convenient, this collision is expressed by the symbol 1–1 → 1–1 here.

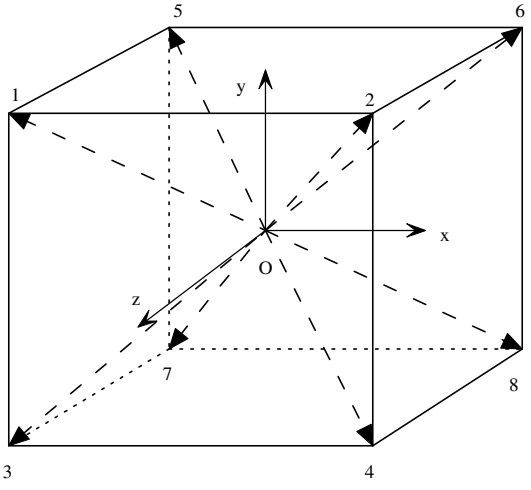

Fig. 1. Discrete velocity direction model.

(2) Included angles are equal to $2\text{arctg}(\sqrt{2}/2)$. There is only one scattering way for this kind of collisions in order to satisfy the law of conservation of momentum, namely molecules change their velocities with each other after collision. The collisions with the molecules in directions 2, 3 and 5 can be expressed by 1–2 → 2–1, 1–3 → 3–1 and 1–5 → 5–1.
(3) Included angles are equal to $2\text{arctg}\sqrt{2}$. The scattering way of this collision is just like the second one. The collisions are 1–4 → 4–1, 1–6 → 6–1 and 1–7 → 7–1.
(4) Included angles are equal to π. There is only one scattering way that can satisfy the laws of conservation of energy and momentum simultaneously for this collision because two molecules have different speed rates. Namely, two molecules will move oppositely and change their speed rates, 1–8 → 8–1.

Besides the binary collisions, there is a kind of multi-body collisions that can easily satisfy the laws of conservation of energy and momentum simultaneously in this model. The total momentum can be conservative when some couples of molecules in a diagonal line scatter into other three diagonal lines in pairs by different probabilities if all molecular couples change their speeds after collision. Consider N molecular couples of 1–8 in a finite volume (the molecular rate of speed in the first direction is c_a and the rate of speed in the second direction is c_b in all symbols). There are six feasible scattering ways: 1–8 → 2–7, 1–8 → 7–2, 1–8 → 3–6, 1–8 → 6–3, 1–8 → 4–5, 1–8 → 5–4. These ways may be classified into two groups by scattering angles:

Group 1: 1–8 → 2–7 1–8 → 3–6 1–8 → 5–4
Group 2: 1–8 → 7–2 1–8 → 6–3 1–8 → 4–5

The scattering ways in each group should have the same probability because they have equal angles. We assume that the probability of the first group is α and that of the second group is β. Then the law of conservation of mass can be written as

$$3\alpha + 3\beta = 1. \tag{3}$$

According to the law of conservation of momentum, the other relationship between α and β can be written as

$$-\alpha + \beta = 1. \tag{4}$$

Solving Eqs. (3) and (4), then

$$\alpha = -\frac{1}{3}, \tag{5}$$

$$\beta = \frac{2}{3}. \tag{6}$$

The value of probability α is negative here. So we must amend the description of this kind of collisions. The negative probability α implies that the number of molecules with speed c_b in directions 2, 3, 5 and the number of molecules with speed c_a in directions 7, 6, 4 decrease after collision. These losing molecules can be taken as those that participate in the multi-body collision. Then we re-define this multi-body collision: three molecular couples 1–8 collide with three molecular couples of 2–7, 3–6, 5–4. After collision, these molecular couples scatter into directions 7–2, 6–3, 4–5 averagely. Then Eqs. (3) and (4) should be written as $3\beta = 1 + 3\alpha$ and $\alpha + \beta = 1$. Therefore, two probabilities are $\alpha = 1/3$ and $\beta = 2/3$. Now, this collision can be described by the following symbol:

$$3(1\text{–}8) + (7\text{–}2) + (6\text{–}3) + (4\text{–}5) \rightarrow 2(2\text{–}7) + 2(3\text{–}6) + 2(5\text{–}4).$$

According to the characteristic of centrosymmetry, the kind of multi-body collisions in other directions can be described by the following symbols:

$$3(8\text{–}1) + (2\text{–}7) + (3\text{–}6) + (5\text{–}4) \rightarrow 2(7\text{–}2) + 2(6\text{–}3) + 2(4\text{–}5),$$
$$3(2\text{–}7) + (8\text{–}1) + (3\text{–}6) + (5\text{–}4) \rightarrow 2(1\text{–}8) + 2(6\text{–}3) + 2(4\text{–}5),$$
$$3(7\text{–}2) + (1\text{–}8) + (6\text{–}3) + (4\text{–}5) \rightarrow 2(8\text{–}1) + 2(3\text{–}6) + 2(5\text{–}4),$$
$$3(3\text{–}6) + (2\text{–}7) + (8\text{–}1) + (5\text{–}4) \rightarrow 2(7\text{–}2) + 2(1\text{–}8) + 2(4\text{–}5),$$

$$3(6\text{–}3) + (7\text{–}2) + (1\text{–}8) + (4\text{–}5) \rightarrow 2(2\text{–}7) + 2(8\text{–}1) + 2(5\text{–}4),$$
$$3(4\text{–}5) + (7\text{–}2) + (6\text{–}3) + (1\text{–}8) \rightarrow 2(2\text{–}7) + 2(3\text{–}6) + 2(8\text{–}1),$$
$$3(5\text{–}4) + (2\text{–}7) + (3\text{–}6) + (8\text{–}1) \rightarrow 2(7\text{–}2) + 2(6\text{–}3) + 2(1\text{–}8),$$

2.4. Statistics of collisions

According to the above analysis, the speed distribution functions will only be changed by the multi-body collisions in the present model. Consider the speed distribution function in direction 1 first. The multi-body collisions 1–8, 7–2, 6–3 and 4–5 will reduce the number of molecules with speed c_a, on the other hand the multi-body collisions 2–7, 3–6 and 5–4 will increase it. During a time interval $\mathrm{d}t$, the number of collisions between the molecules with speed c_a in direction 1 and all molecules in direction 8 is

$$\pi d^2 \,\mathrm{d}\vec{r}\,\mathrm{d}t\,\mathrm{d}c_a \int_0^\infty (c_a + c_b) f_8(c_b, \vec{r}, t) f_1(c_a, \vec{r}, t)\,\mathrm{d}c_b,$$

in which d is the molecular diameter. These collisions may include both the binary collisions and the multi-body collisions. Let C be the ratio of multi-body collisions, then the losing number by this kind of multi-body collisions can be written as

$$C\pi d^2 \,\mathrm{d}\vec{r}\,\mathrm{d}t\,\mathrm{d}c_a \int_0^\infty (c_a + c_b) f_8(c_b, \vec{r}, t) f_1(c_a, \vec{r}, t)\,\mathrm{d}c_b.$$

In the same way, the losing number of molecules with speed c_a in direction 1 causing by the multi-body collisions 7–2, 6–3 and 4–5 can be written as

$$7\text{–}2: \quad \frac{C}{3}\pi d^2 \,\mathrm{d}\vec{r}\,\mathrm{d}t\,\mathrm{d}c_a \int_0^\infty (c_a + c_b) f_2(c_b, \vec{r}, t) f_7(c_a, \vec{r}, t)\,\mathrm{d}c_b,$$
$$6\text{–}3: \quad \frac{C}{3}\pi d^2 \,\mathrm{d}\vec{r}\,\mathrm{d}t\,\mathrm{d}c_a \int_0^\infty (c_a + c_b) f_3(c_b, \vec{r}, t) f_6(c_a, \vec{r}, t)\,\mathrm{d}c_b,$$
$$4\text{–}5: \quad \frac{C}{3}\pi d^2 \,\mathrm{d}\vec{r}\,\mathrm{d}t\,\mathrm{d}c_a \int_0^\infty (c_a + c_b) f_5(c_b, \vec{r}, t) f_4(c_a, \vec{r}, t)\,\mathrm{d}c_b.$$

Add these terms together and divide them by term $\mathrm{d}\vec{r}\mathrm{d}C_a\,\mathrm{d}t$, then the expression of the losing term in direction 1 can be written as

$$L_1 = C\pi d^2 \left[\int_0^\infty (c_a + c_b) f_8(c_b, \vec{r}, t) f_1(c_a, \vec{r}, t)\,\mathrm{d}c_b + \frac{1}{3}\int_0^\infty (c_a + c_b) f_2(c_b, \vec{r}, t) f_7(c_a, \vec{r}, t)\,\mathrm{d}c_b \right.$$
$$\left. + \frac{1}{3}\int_0^\infty (c_a + c_b) f_3(c_b, \vec{r}, t) f_6(c_a, \vec{r}, t)\,\mathrm{d}c_b + \frac{1}{3}\int_0^\infty (c_a + c_b) f_5(c_b, \vec{r}, t) f_4(c_a, \vec{r}, t)\,\mathrm{d}c_b \right]. \tag{7}$$

Then the gaining term in direction 1 is

$$G_1 = \frac{2}{3} C\pi d^2 \left[\int_0^\infty (c_a + c_b) f_7(c_b, \vec{r}, t) f_2(c_a, \vec{r}, t)\,\mathrm{d}c_b + \int_0^\infty (c_a + c_b) f_6(c_b, \vec{r}, t) f_3(c_a, \vec{r}, t)\,\mathrm{d}c_b \right.$$
$$\left. + \int_0^\infty (c_a + c_b) f_4(c_b, \vec{r}, t) f_5(c_a, \vec{r}, t)\,\mathrm{d}c_b \right]. \tag{8}$$

Now, we gained the expressions of collision term in direction 1. Expressions in other directions can be written as follows in the same manner:

Direction 2:

$$L_2 = C\pi d^2 \left[\int_0^\infty (c_a + c_b) f_7(c_b, \vec{r}, t) f_2(c_a, \vec{r}, t)\,\mathrm{d}c_b + \frac{1}{3}\int_0^\infty (c_a + c_b) f_1(c_b, \vec{r}, t) f_8(c_a, \vec{r}, t)\,\mathrm{d}c_b \right.$$
$$\left. + \frac{1}{3}\int_0^\infty (c_a + c_b) f_4(c_b, \vec{r}, t) f_5(c_a, \vec{r}, t)\,\mathrm{d}c_b + \frac{1}{3}\int_0^\infty (c_a + c_b) f_6(c_b, \vec{r}, t) f_3(c_a, \vec{r}, t)\,\mathrm{d}c_b \right] \tag{9}$$

$$G_2 = \frac{2}{3}C\pi d^2\left[\int_0^\infty (c_a + c_b) f_8(c_b,\vec{r},t) f_1(c_a,\vec{r},t)\,\mathrm{d}c_b + \int_0^\infty (c_a + c_b) f_5(c_b,\vec{r},t) f_4(c_a,\vec{r},t)\,\mathrm{d}c_b + \int_0^\infty (c_a + c_b) f_3(c_b,\vec{r},t) f_6(c_a,\vec{r},t)\,\mathrm{d}c_b\right]. \tag{10}$$

Direction 3:

$$L_3 = C\pi d^2\left[\int_0^\infty (c_a + c_b) f_6(c_b,\vec{r},t) f_3(c_a,\vec{r},t)\,\mathrm{d}c_b + \frac{1}{3}\int_0^\infty (c_a + c_b) f_1(c_b,\vec{r},t) f_8(c_a,\vec{r},t)\,\mathrm{d}c_b + \frac{1}{3}\int_0^\infty (c_a + c_b) f_4(c_b,\vec{r},t) f_5(c_a,\vec{r},t)\,\mathrm{d}c_b + \frac{1}{3}\int_0^\infty (c_a + c_b) f_7(c_b,\vec{r},t) f_2(c_a,\vec{r},t)\,\mathrm{d}c_b\right] \tag{11}$$

$$G_3 = \frac{2}{3}C\pi d^2\left[\int_0^\infty (c_a + c_b) f_8(c_b,\vec{r},t) f_1(c_a,\vec{r},t)\,\mathrm{d}c_b + \int_0^\infty (c_a + c_b) f_5(c_b,\vec{r},t) f_4(c_a,\vec{r},t)\,\mathrm{d}c_b + \int_0^\infty (c_a + c_b) f_2(c_b,\vec{r},t) f_7(c_a,\vec{r},t)\,\mathrm{d}c_b\right]. \tag{12}$$

Direction 4:

$$L_4 = C\pi d^2\left[\int_0^\infty (c_a + c_b) f_5(c_b,\vec{r},t) f_4(c_a,\vec{r},t)\,\mathrm{d}c_b + \frac{1}{3}\int_0^\infty (c_a + c_b) f_2(c_b,\vec{r},t) f_7(c_a,\vec{r},t)\,\mathrm{d}c_b + \frac{1}{3}\int_0^\infty (c_a + c_b) f_3(c_b,\vec{r},t) f_6(c_a,\vec{r},t)\,\mathrm{d}c_b + \frac{1}{3}\int_0^\infty (c_a + c_b) f_8(c_b,\vec{r},t) f_1(c_a,\vec{r},t)\,\mathrm{d}c_b\right]. \tag{13}$$

$$G_4 = \frac{2}{3}C\pi d^2\left[\int_0^\infty (c_a + c_b) f_7(c_b,\vec{r},t) f_2(c_a,\vec{r},t)\,\mathrm{d}c_b + \int_0^\infty (c_a + c_b) f_6(c_b,\vec{r},t) f_3(c_a,\vec{r},t)\,\mathrm{d}c_b + \int_0^\infty (c_a + c_b) f_1(c_b,\vec{r},t) f_8(c_a,\vec{r},t)\,\mathrm{d}c_b\right]. \tag{14}$$

Direction 5:

$$L_5 = C\pi d^2\left[\int_0^\infty (c_a + c_b) f_4(c_b,\vec{r},t) f_5(c_a,\vec{r},t)\,\mathrm{d}c_b + \frac{1}{3}\int_0^\infty (c_a + c_b) f_1(c_b,\vec{r},t) f_8(c_a,\vec{r},t)\,\mathrm{d}c_b + \frac{1}{3}\int_0^\infty (c_a + c_b) f_6(c_b,\vec{r},t) f_3(c_a,\vec{r},t)\,\mathrm{d}c_b + \frac{1}{3}\int_0^\infty (c_a + c_b) f_7(c_b,\vec{r},t) f_2(c_a,\vec{r},t)\,\mathrm{d}c_b\right]. \tag{15}$$

$$G_5 = \frac{2}{3}C\pi d^2\left[\int_0^\infty (c_a + c_b) f_8(c_b,\vec{r},t) f_1(c_a,\vec{r},t)\,\mathrm{d}c_b + \int_0^\infty (c_a + c_b) f_3(c_b,\vec{r},t) f_6(c_a,\vec{r},t)\,\mathrm{d}c_b + \int_0^\infty (c_a + c_b) f_2(c_b,\vec{r},t) f_7(c_a,\vec{r},t)\,\mathrm{d}c_b\right]. \tag{16}$$

Direction 6:

$$L_6 = C\pi d^2\left[\int_0^\infty (c_a + c_b) f_3(c_b,\vec{r},t) f_6(c_a,\vec{r},t)\,\mathrm{d}c_b + \frac{1}{3}\int_0^\infty (c_a + c_b) f_2(c_b,\vec{r},t) f_7(c_a,\vec{r},t)\,\mathrm{d}c_b + \frac{1}{3}\int_0^\infty (c_a + c_b) f_5(c_b,\vec{r},t) f_4(c_a,\vec{r},t)\,\mathrm{d}c_b + \frac{1}{3}\int_0^\infty (c_a + c_b) f_8(c_b,\vec{r},t) f_1(c_a,\vec{r},t)\,\mathrm{d}c_b\right]. \tag{17}$$

$$G_6 = \frac{2}{3}C\pi d^2\left[\int_0^\infty (c_a + c_b) f_7(c_b,\vec{r},t) f_2(c_a,\vec{r},t)\,\mathrm{d}c_b + \int_0^\infty (c_a + c_b) f_4(c_b,\vec{r},t) f_5(c_a,\vec{r},t)\,\mathrm{d}c_b + \int_0^\infty (c_a + c_b) f_1(c_b,\vec{r},t) f_8(c_a,\vec{r},t)\,\mathrm{d}c_b\right]. \tag{18}$$

Direction 7:

$$L_7 = C\pi d^2\left[\int_0^\infty (c_a+c_b)f_2(c_b,\vec{r},t)f_7(c_a,\vec{r},t)\,\mathrm{d}c_b + \frac{1}{3}\int_0^\infty (c_a+c_b)f_3(c_b,\vec{r},t)f_6(c_a,\vec{r},t)\,\mathrm{d}c_b + \frac{1}{3}\int_0^\infty (c_a+c_b)f_5(c_b,\vec{r},t)f_4(c_a,\vec{r},t)\,\mathrm{d}c_b + \frac{1}{3}\int_0^\infty (c_a+c_b)f_8(c_b,\vec{r},t)f_1(c_a,\vec{r},t)\,\mathrm{d}c_b\right]. \tag{19}$$

$$G_7 = \frac{2}{3}C\pi d^2\left[\int_0^\infty (c_a+c_b)f_6(c_b,\vec{r},t)f_3(c_a,\vec{r},t)\,\mathrm{d}c_b + \int_0^\infty (c_a+c_b)f_4(c_b,\vec{r},t)f_5(c_a,\vec{r},t)\,\mathrm{d}c_b + \int_0^\infty (c_a+c_b)f_1(c_b,\vec{r},t)f_8(c_a,\vec{r},t)\,\mathrm{d}c_b\right]. \tag{20}$$

Direction 8:

$$L_8 = C\pi d^2\left[\int_0^\infty (c_a+c_b)f_1(c_b,\vec{r},t)f_8(c_a,\vec{r},t)\,\mathrm{d}c_b + \frac{1}{3}\int_0^\infty (c_a+c_b)f_4(c_b,\vec{r},t)f_5(c_a,\vec{r},t)\,\mathrm{d}c_b + \frac{1}{3}\int_0^\infty (c_a+c_b)f_6(c_b,\vec{r},t)f_3(c_a,\vec{r},t)\,\mathrm{d}c_b + \frac{1}{3}\int_0^\infty (c_a+c_b)f_7(c_b,\vec{r},t)f_2(c_a,\vec{r},t)\,\mathrm{d}c_b\right]. \tag{21}$$

$$G_8 = \frac{2}{3}C\pi d^2\left[\int_0^\infty (c_a+c_b)f_5(c_b,\vec{r},t)f_4(c_a,\vec{r},t)\,\mathrm{d}c_b + \int_0^\infty (c_a+c_b)f_3(c_b,\vec{r},t)f_6(c_a,\vec{r},t)\,\mathrm{d}c_b + \int_0^\infty (c_a+c_b)f_2(c_b,\vec{r},t)f_7(c_a,\vec{r},t)\,\mathrm{d}c_b\right] \tag{22}$$

The form of these governing equations is an intermediate between the Boltzmann equation and the equations of the conventional discrete velocity models. They are all differential-integral equations and include the products of unknown variables in the integral terms. So there is no reduction in mathematic difficulty and analytic solution still cannot be obtained for most flow situations. But the variables of these equations are three-dimensional, instead of the six-dimensional velocity distribution function in the Boltzmann equation. By getting rid of three dimensions, the computational cost can be reduced greatly.

3. Numerical calculations and discussion

In this section, the Couette flow and Poiseuille flow are investigated, which have been widely used as benchmark problems to test new analytical and numerical methods. For two flows, the Knudsen number is defined as the ratio of the molecular mean free path (λ) to the distance (H) between two plates, $Kn = \lambda/H$. The molecular mean free path is derived by the hard sphere mode, $\lambda = (\sqrt{2}\pi d^2 n)^{-1}$. These calculations range from the continuum regime to the transition regime ($0.01 \leqslant Kn \leqslant 10$), which cover most gas flows in MEMS. The grids are uniform and the space step length is less than the mean free path in all calculations.

The finite difference method of second-order upwind scheme is employed as the numerical method in the paper. The Couette flow and Poiseuille flow are both steady flows, namely $\frac{\partial f_i}{\partial t} = 0$. So the unsteady terms in these governing equations are vanished, only the convection terms are left on the left hand sides. The integral terms on the right-hand side will be replaced by some product terms of unknown variables after integration. The discrete values of speed rate were obtained by the following steps in the present calculations:

(1) Divide the speed space into N interval: $[0, c_1)$, $[c_1, c_2), \ldots, [c_{N-1}, \infty)$.
(2) The average values of speed rate in each interval are taken as the discrete values. The average values in speed interval j can be obtained by the following equation at the intervals from 1 to $N-1$.

$$\overline{c_j} = \frac{\int_{c_{j-1}}^{c_j} f^{\mathrm{eq}} c\,\mathrm{d}c}{\int_{c_{j-1}}^{c_j} f^{\mathrm{eq}}\,\mathrm{d}c}, \tag{23}$$

in which f^{eq} is the Maxwell distribution, $f^{\mathrm{eq}} = n(\frac{m}{2\pi kT})^{\frac{3}{2}} \mathrm{e}^{-\frac{mC^2}{2kT}}$. In the last speed interval, the speed is infinite. The average rate of speed can be obtained by the following method:

$$\overline{c_N} = \frac{\overline{C} - \sum_{j=1}^{N-1} \int_{c_{j-1}}^{c_j} f^{eq} c \, dc}{1 - \sum_{j=1}^{N-1} \int_{c_{j-1}}^{c_j} f^{eq} \, dc}. \tag{24}$$

The speed rate of molecular mean thermal motion $\overline{C}$ is obtained by $\overline{C} = \sqrt{8kT/\pi m}$, in which k is the Boltzmann constant, m is the molecular mass. We chose eight discrete values of speed rate in the present calculations. Then there are 64 discrete velocities together in eight directions. By the integration of 8 discrete equations in 8 speed intervals, we can obtain 64 difference equations, in which the integral terms on the right-hand side were replaced by the product terms.

Here, the Maxwell distribution $f^{eq} = n(\frac{m}{2\pi kT})^{\frac{3}{2}} e^{-\frac{mC^2}{2kT}}$ is employed. To test that it is the equilibrium state distribution of the present collision operator, a Couette flow was calculated here. This calculation started from a non-Maxwell distribution. The gas between two plates is argon and wall temperature is 273 K. Eight speeds were chosen in this calculation. Eight speed values are 81.91 m/s, 174.07 m/s, 277.46 m/s, 383.45 m/s, 490.37 m/s, 597.75 m/s, 705.40 m/s, 843.01 m/s. At the beginning, all molecular speeds are equal to 81.91 m/s. Results in the middle of the channel are compared with the Maxwell distribution, which are shown in Table 1. The results show that the Maxwell distribution is an attracting fixed point for the present collision operator.

Collisions between molecules and walls are very complicated. Up to now, there is no precise method in both theory and experiment. So some approximate model are usually used, such as the direct reflection model, the diffuse reflect model, the Maxwell model, the CLL model that is widely used in the DSMC method and so on [2,9,10,12]. In this paper, the diffuse reflection model was employed. It is shown in Fig. 2.

The molecules in directions 3, 4, 7 and 8 move towards the wall and these molecules reflect into directions 1, 2, 5 and 6 averagely. The molecular number density in direction i with speed rate c_j can be obtained by the following equation:

$$n_{i,j} = \frac{1}{4}(n_3 + n_4 + n_7 + n_8)P_j, \tag{25}$$

in which P_j is equal to $\int_{c_{j-1}}^{c_j} f^{eq} \, dc$ when $1 \leqslant i \leqslant N-1$ and equal to $1 - \sum_{j=1}^{N-1} \int_{c_{j-1}}^{c_j} f^{eq} \, dc$ when $j = N$ (the f^{eq} is the Maxwell distribution at wall temperature.).

Table 1
Test of equilibrium state distribution

	Speed distributions							
Speed (m/s)	81.91	174.07	277.46	383.45	490.37	597.75	705.40	843.01
Maxwell	0.0245	0.1384	0.2471	0.2569	0.1834	0.0961	0.0382	0.0152
Direction 1	0.0243	0.1373	0.2458	0.2566	0.1842	0.0972	0.0389	0.0156
Direction 2	0.0243	0.1373	0.2458	0.2566	0.1842	0.0972	0.0389	0.0156
Direction 3	0.0243	0.1373	0.2458	0.2566	0.1842	0.0972	0.0389	0.0156
Direction 4	0.0243	0.1373	0.2458	0.2566	0.1842	0.0972	0.0389	0.0156
Direction 5	0.0243	0.1373	0.2458	0.2566	0.1842	0.0972	0.0389	0.0156
Direction 6	0.0243	0.1373	0.2458	0.2566	0.1842	0.0972	0.0389	0.0156
Direction 7	0.0243	0.1373	0.2458	0.2566	0.1842	0.0972	0.0389	0.0156
Direction 8	0.0243	0.1373	0.2458	0.2566	0.1842	0.0972	0.0389	0.0156

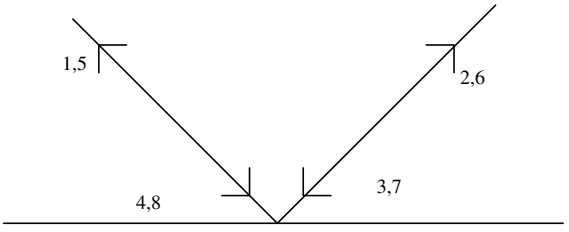

Fig. 2. Wall collision.

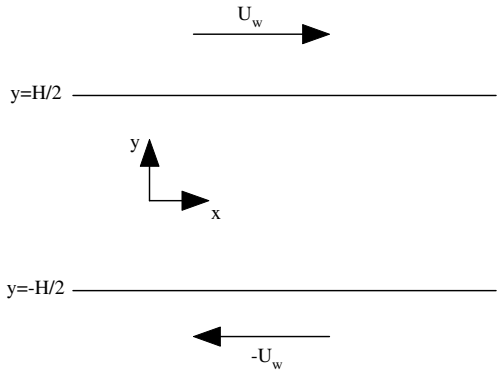

Fig. 3. Couette flow.

Table 2
The rate of change of C versus various values of Kn and U_w

	$\frac{C_m - C_w}{C_w}$			
Kn	U_w (m/s) 0.1	1	10	100
0.01	0.1575%	0.0197%	0.0025%	0.1770%
0.1	0.0025%	0.0101%	0.0010%	0.0049%
1	0	0	0	0

The coefficient C in eight governing equations is the ratio of multi-body collisions. According to the above analysis, only the multi-body collisions can alter the speed distribution functions in the present model. Therefore, gas state is easy to be altered at large C because more molecules can participate the multi-body collisions. Namely, the viscosity coefficient decreases when the coefficient C increases. The value of the coefficient C can be determined by the viscosity coefficient in the Couette flow:

(1) Assign an initial value to the coefficient C.
(2) Calculate the horizontal velocity u and the shearing stress τ in the Couette flow (Fig. 3), in which the Knudsen number, temperature and pressure are equal to the given values.
(3) Calculate the viscosity coefficient μ by the equation $\tau = -\mu \frac{du}{dy}$.
(4) Compared μ with the given viscosity coefficient μ^*. If $\mu > \mu^*$, increase the value of C and if $\mu < \mu^*$, decrease the value of C.
(5) Return to the step 2 until $|\mu - \mu^*| < \varepsilon$, in which ε is a small positive value.

The coefficient C is a function of flow conditions, such as the Knudsen number, the speed number, gas temperature and so on. Therefore it will change with flow conditions. The study on the change of coefficient C in the Couette flow is shown in Table 2. In these calculations, the Knudsen number ranges from 0.01 to 1 and the plate velocity (U_w) ranges from 0.1 m/s to 100 m/s. The gas between two plates is argon. Pressure is equal to 101325 Pa and the wall temperature is equal to 273 K. C_w is the value of coefficient C on the upper wall and C_m is the value of coefficient C in the middle of the channel. The rate of change of C is $\frac{C_m - C_w}{C_w}$.

The results show that the change of C is very small. The largest value in all calculations is 0.177%. So the coefficient C was considered as a constant in the following calculations.

3.1. Couette flow

The Couette flow is a kind of steady flow that is driven by the surface stress of two infinite and parallel plates moving oppositely along their own planes, which is shown in Fig. 3.

Table 3
The distributions of dimensionless velocity u/U_w versus various values of Kn ($0.01 \leqslant Kn < 0.1$) in the upper half channel of the Couette flow

y	u/U_w								
	$Kn = 0.01$	0.02	0.03	0.04	0.05	0.06	0.07	0.08	0.09
0.00	0.0031	0.0007	0.0003	0.0000	0.0000	0.0000	0.0000	0.0000	0.0000
0.05	0.0956	0.0967	0.0959	0.0949	0.0937	0.0926	0.0915	0.0904	0.0893
0.10	0.1944	0.1941	0.1921	0.1898	0.1875	0.1852	0.1829	0.1807	0.1785
0.15	0.2932	0.2916	0.2883	0.2848	0.2813	0.2778	0.2744	0.2711	0.2678
0.20	0.3921	0.3891	0.3845	0.3798	0.3751	0.3704	0.3659	0.3614	0.3571
0.25	0.4911	0.4865	0.4807	0.4747	0.4689	0.4631	0.4574	0.4518	0.4463
0.30	0.5901	0.5840	0.5769	0.5697	0.5626	0.5557	0.5488	0.5422	0.5356
0.35	0.6893	0.6816	0.6731	0.6647	0.6564	0.6483	0.6403	0.6325	0.6249
0.40	0.7884	0.7791	0.7693	0.7597	0.7502	0.7409	0.7318	0.7229	0.7142
0.45	0.8876	0.8766	0.8655	0.8546	0.8440	0.8335	0.8233	0.8132	0.8034
0.50	0.9867	0.9741	0.9617	0.9496	0.9378	0.9261	0.9148	0.9036	0.8927

Table 4
The distributions of dimensionless velocity u/U_w versus various values of Kn ($0.1 \leqslant Kn < 1$) in the upper half channel of the Couette flow

	u/U_w								
y	$Kn = 0.1$	0.2	0.3	0.4	0.5	0.6	0.7	0.8	0.9
0.00	0.0000	0.0000	0.0000	0.0000	0.0000	0.0000	0.0000	0.0000	0.0000
0.05	0.0882	0.0786	0.0708	0.0644	0.0589	0.0543	0.0504	0.0469	0.0439
0.10	0.1764	0.1573	0.1417	0.1287	0.1179	0.1086	0.1007	0.0939	0.0879
0.15	0.2646	0.2359	0.2125	0.1931	0.1768	0.1630	0.1511	0.1408	0.1318
0.20	0.3528	0.3146	0.2833	0.2574	0.2357	0.2173	0.2015	0.1878	0.1758
0.25	0.4410	0.3932	0.3541	0.3218	0.2947	0.2716	0.2518	0.2347	0.2197
0.30	0.5292	0.4719	0.4250	0.3862	0.3536	0.3260	0.3022	0.2816	0.2636
0.35	0.6774	0.5505	0.4958	0.4505	0.4125	0.3803	0.3526	0.3286	0.3076
0.40	0.7056	0.6292	0.5667	0.5149	0.4714	0.4346	0.4029	0.3755	0.3515
0.45	0.7938	0.7078	0.6375	0.5793	0.5304	0.4889	0.4533	0.4225	0.3954
0.50	0.8820	0.7865	0.7083	0.6436	0.5893	0.5432	0.5037	0.4693	0.4394

Table 5
The average values of horizontal shearing stress versus various Kn

Kn	Tao (N/m^2)	Kn	Tao (N/m^2)
0.01	0.6694	0.1	5.974
0.02	1.320	0.2	10.66
0.03	1.955	0.3	14.39
0.04	2.573	0.4	17.84
0.05	3.176	0.5	19.96
0.06	3.764	0.6	22.08
0.07	4.337	0.7	23.88
0.08	4.897	0.8	25.44
0.09	5.442	0.9	26.78

The numerical results of argon with temperature and pressure of 273 K and 101325 Pa are shown in Tables 3–5 and Figs. 4 and 5. The molecular diameter of argon is $d = 3.659 \times 10^{-10}$ m and the viscosity coefficient is $\mu = 2.117 \times 10^{-5}$ Ns/m^{-2}. In these calculations, the plate velocity U_w is equal to 0.1 m/s. The dimensionless velocity distributions in the upper half channel versus various Knudsen number are given in Tables 3 and 4. These velocity distributions are linear and all have discontinuities on the plates. The slippage increases with the growing of Knudsen number. In the continuum regime ($Kn = 0.01$), the velocity on the plate surface is about $0.9867U_w$, which is very close to the plate velocity. In the transition regime, the velocity on the plate

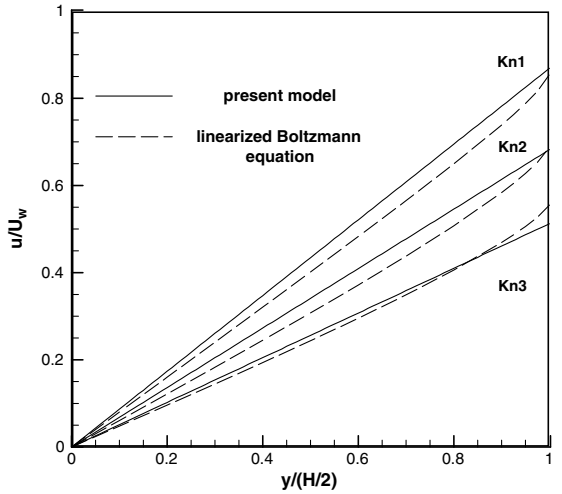

Fig. 4. Comparison of velocity profiles in the upper half channel with those by the linearized Boltzmann equation.

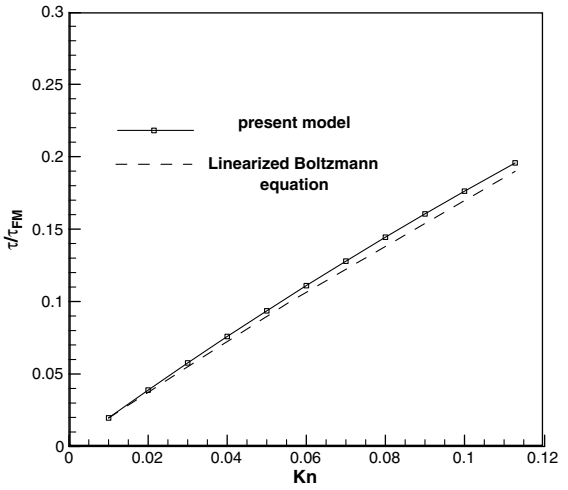

Fig. 5. The shearing stress versus the Knudsen number in Couette flow.

surface is only $0.4394U_{\mathrm{w}}$. Comparing the results of the linearized Boltzmann equation [18] and the DSMC method (IP), the errors are less than 2% while $0.01 < Kn < 0.1$ and less than 6% while $0.1 < Kn < 1$.

Profiles of dimensionless velocity distributions in the upper half channel compared to the results of the linearized Boltzmann equation at three Knudsen number ($Kn1 = 0.1128$, $Kn2 = 0.3385$ and $Kn3 = 0.6770$) are shown in Fig. 4 (The compared data is from Ref. [18]). The linear degree of the present results is better than that of the linearized Boltzmann equation and the profiles of the two methods differ not much from each other.

The average values of horizontal shearing stress versus various Knudsen number are given in Table 5. The shearing stress will increase while the Knudsen number grows. The phenomena can be explained by the equation $\tau = -\mu\frac{\mathrm{d}u}{\mathrm{d}h}$. According to the above results of velocity distributions, the distance between two parallel plates decreases faster than the horizontal velocity with the increasing of the Knudsen number.

The relation of the shearing stress versus the Knudsen number comparing with the results by the Linearized Boltzmann equation is given in Fig. 5. The normalization factor is the collisionless solution of shearing stress, $\tau_{FM} = mnc_{\mathrm{m}}U_{\mathrm{w}}/\sqrt{\pi}$, in which c_{m} is the most probable speed rate. Present profiles agree well with the results by the linearized Boltzmann equation. The error is less than 3%.

Table 6
Molecular diameters and viscosity coefficients of five gases at temperature of 273 K

	He	Ar	N_2	O_2	CO_2
Diameter ($d \times 10^{10}$ m)	2.193	3.659	3.784	3.636	4.643
Viscosity ($\mu \times 10^5$ Ns/m^2)	1.865	2.117	1.656	1.919	1.380

Table 7
Shearing stress of five kinds of gases of Couette flow

	Shear stress (N/m^2)				
	He	Ar	N_2	O_2	CO_2
Present	1.0561	3.3365	2.7821	2.9815	3.5149
DSMC	1.0300	3.2411	2.7262	3.1517	3.4068
IP	1.0447	3.2515	2.6936	2.9227	3.4461

The shearing stress of five kinds of gases was calculated here. These gases are He, Ar, N_2, O_2 and CO_2 with the pressure and temperature of 1013.25 Pa and 273 K. The Knudsen number is 0.01. The values of diameters and viscosity coefficients are obtained from the experimental data of Ref. [10], which are shown in Table 6.

The values of shearing stress are given in Table 7. The compared results by the DSMC method and the IP method were calculated under the same conditions. The result by IP method is from Ref. [2]. Errors of five gases compared with other methods are very small.

To our knowledge, the discrete velocity models will fail at very high speed flows and they deviate clearly from the Boltzmann equation at large Knudsen number [31–34]. The present model meets these problems, too. The limiting flow speed in the Couette flow was studied in Table 8. In these calculations, the plate velocities U_w range from 1 m/s to 600 m/s. The gas between two plates is argon. The Knudsen number is 0.1, the temperature is 273 K and the pressure is 101325 Pa. The sonic speed is 282.05 m/s under these conditions. These calculations show that the results will be divergent when plate velocity is larger than 600 m/s. Namely, the present model is not valid. When the plate speeds are less then 500 m/s, the change of dimensionless velocities is slight. The largest error is less than 3%.

Dimensionless distributions of velocity of the Couette flow at large Kundsen number ($Kn1 = 2.257$ and $Kn2 = 4.51352$) are shown in Fig. 6. In these calculations, the gas is still argon, the plate temperature is 273 K, the pressure is 101325 Pa and the wall speed is 0.1 m/s. The results show that the present model deviate clearly from the linearized Boltzmann equation at these Knudsen number and the error increases with the growing of the Knudsen number. This phenomenon is similar to that in the Broadwell model. The reason is that the number of velocities is finite in these discrete models, which brings error. At small Knudsen number, the collision between molecules is frequent so that the error falls rapidly. But at large Knudsen number, the collision between molecules becomes weak. Then the error becomes clearly.

The speed number in the present model may vary. Dimensionless velocities on the upper plate under various speeds were calculated in Table 9. In these calculations, the gas is argon, $Kn = 0.3385$, temperature = 273 K, pressure=101325 Pa and $U_w = 1$ m/s. 8, 16, 32 and 64 speeds were employed. The results were compared to that by the linearized Boltzmann equation. These results show that the precision of dimensionless velocities increases with the increasing of speed number. But the increasing of precision is slower than the increasing of the computational cost.

Table 8
Dimensionless velocities with various plate speeds

U_w (m/s)	1.0	10	100	200
u/U_w	0.8820	0.8820	0.8829	0.8857
U_w (m/s)	300	400	500	600
u/U_w	0.8883	0. 8847	0.8674	Divergence

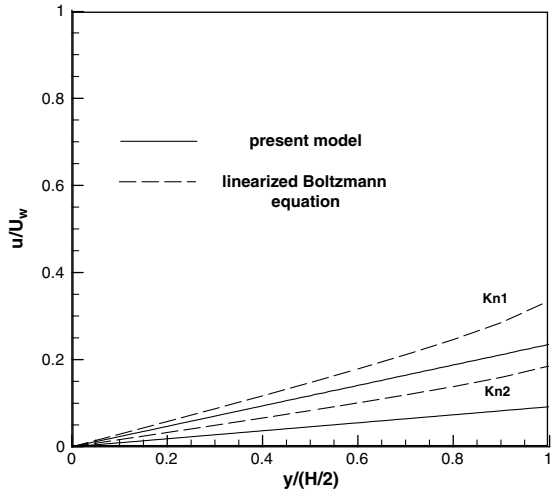

Fig. 6. Comparison of velocity profiles in the upper half channel with those by the linearized Boltzmann equation.

Table 9
Dimensionless velocities under various speed number

Speed number	8	16	32	64	Linearized
u/U_w	0.6821	0.6829	0.6831	0.6831	0.6874

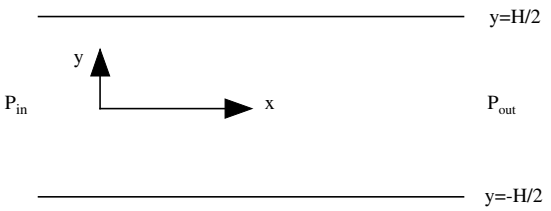

Fig. 7. Poiseuille flow.

Table 10
The velocity distributions in the upper half channel for various Kn ($0.01 \leqslant Kn < 0.1$) of Poiseuille flow

	Velocity $u \times 10^2$ m/s								
x	$Kn = 0.01$	0.02	0.03	0.04	0.05	0.06	0.07	0.08	0.09
0.00	8.057	4.369	3.047	2.363	1.946	1.663	1.459	1.304	1.184
0.05	7.978	4.328	3.018	2.342	1.929	1.648	1.446	1.293	1.174
0.10	7.742	4.202	2.933	2.277	1.877	1.605	1.409	1.261	1.145
0.15	7.348	3.994	2.791	2.169	1.790	1.532	1.347	1.206	1.097
0.20	6.797	3.702	2.592	2.019	1.669	1.431	1.259	1.130	1.029
0.25	6.088	3.327	2.336	1.825	1.513	1.300	1.147	1.032	0.942
0.30	5.222	2.868	2.024	1.588	1.322	1.141	1.010	0.912	0.835
0.35	4.199	2.326	1.654	1.308	1.096	0.952	0.849	0.770	0.709
0.40	3.018	1.700	1.228	0.984	0.836	0.735	0.662	0.607	0.564
0.45	1.679	0.991	0.745	0.618	0.541	0.488	0.450	0.422	0.399
0.50	0.189	0.201	0.206	0.210	0.212	0.213	0.214	0.215	0.216

3.2. Poiseuille flow

The plane Poiseuille flow is a steady flow that is between two stationary infinite and parallel plates and is driven by a pressure gradient along the plate direction, which is shown in Fig. 7.

The gas between two plates is still argon in the calculations. At inlet, the temperature is 273 K and the pressure P_{in} is 101340.2 Pa. At outlet, the pressure P_{out} is 101309.8 Pa. The ratio of P_{in}/P_{out} is about 1.0003. The first-order derivative of temperature is assumed to be zero at outlet, namely, $\partial T_{out}/\partial x = 0$. The value of temperature of two plates is constant and equals to 273 K.

The velocity distributions in the upper half channel versus various Knudsen number are given in Table 10. The highest value of horizontal velocity is in the middle of the channel and the horizontal velocity slow down near two plates. There is velocity slip on the plates and the slippage increase with the increasing of the Knudsen number.

The profiles at three Knudsen numbers are shown in Fig. 8. At the Knudsen number 0.1128, the velocity distribution was compared with the results of Ohwada [18]. The profiles become smooth as the Knudsen number grows.

The mass fluxes of Poiseuille flow at various Knudsen number are given in Table 11. The results are non-dimensional mass fluxes and the normalization factor is $\frac{mn}{2}\left(\frac{P_{in}-P_{out}}{P_{in}+P_{out}}\right)c_m\frac{h}{L}$, in which L is the length of the channel. These results were compared with those by the Navier–Stokes equation with the slip boundary condition. The

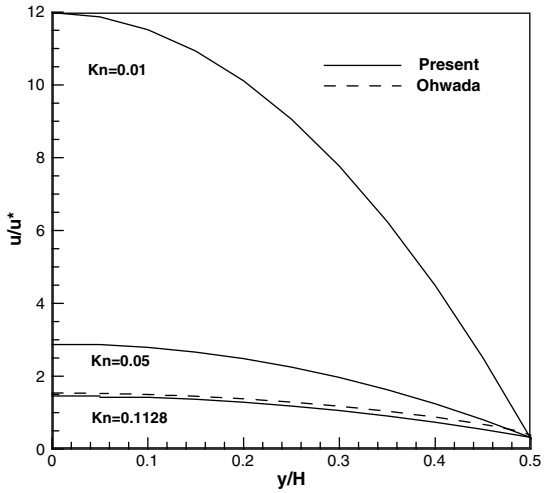

Fig. 8. The velocity distribution in the upper half channel for three Kn numbers.

Table 11
The dimensionless mass fluxes versus the Knudsen number

Kn	$Q/\rho u^* H$	$2(Kn^{-1}+6)/15\sqrt{\pi}$
0.01	8.733	7.97
0.02	4.776	4.21
0.03	3.352	2.96
0.04	2.618	2.33
0.05	2.173	1.96
0.06	1.867	1.71
0.07	1.648	1.53
0.08	1.482	1.39
0.09	1.352	1.29
0.10	1.249	1.2
0.1128	1.142	1.12
0.1128	1.1498	

last result is obtained by the linearized Boltzmann equation [22]. The maximum error compared with those by Navier–Stokes equation is less than 14% and the result (at $Kn = 0.1128$) accord well with that by the linearized Boltzmann equation.

The present calculations were carried out on a 3.0G CPU of Pentium 4. The largest number of points is 1.5×10^5 in all calculations and it needs about 30 h.

4. Conclusions

A discrete velocity direction model for micro gas flows was presented in this paper and it was applied to the low-speed Couette and Poiseuille flows. This method can effectively reduce the numerical calculation cost. The computing speed is about 3 times slower than a NS solver for two dimensional flows when 8 speeds are employed, while the IP method and TPM method are about 10 times slower than a NS solver. Results of velocity distributions, shearing stress and mass fluxes given by the present method agree well with the results of linearized Boltzmann equation and DSMC method (IP).

References

[1] Mohamed Gad-el-Hak, The fluid mechanics of microdevices – the freeman scholar lecture, Journal of Fluids Engineering 121 (1999) 5–32.
[2] Jing Fan, Ching Shen, Statistical simulation of low-speed rarefied gas flows, Journal of Computational Physics 167 (2001) 393–412.
[3] Quanhua Sun, Iain D. Boyd, A direct simulation method for subsonic, microscale gas flows, Journal of Computational Physics 179 (2002) 400–425.
[4] Koji Morinishi, Numerical simulation for gas microflows using Boltzmann equation, Computers & Fluids 35 (2006) 978–985.
[5] J. Pfahler, J.C. Harley, H. Bau, J.N. Zemel, Gas and liquid flow in small channels, ASME-DSC 32 (1991) 49–60.
[6] J.C. Harley, Y. Huang, H. Bau, J.N. Zemel, Gas flow in micro-channels, Journal of Fluid Mechanics 248 (1995) 257–274.
[7] C.M. Ho, Y.C. Tai, Micro-electro-mechanical systems (MEMS) and fluid flows, Annual Review of Fluid Mechanics 30 (1998) 579–612.
[8] Taku Ohwada, Higher order approximation methods for the Boltzmann equation, Journal of Computational Physics 139 (1998) 1–14.
[9] Mikhail N. Kogan, Rarefied Gas Dynamics, Plenum Press, New York, USA, 1969.
[10] S. Chapman, T.G. Cowling, The Mathematical Theory of Non-uniform Gases, Science Press, Beijing, China, 1985.
[11] Q. Shen, Rarefied Gas Dynamics, National Defense Industry Press, Beijing, China, 2003.
[12] G.A. Bird, Molecular Gas Dynamics and the Direct Simulation of Gas Flows, Oxford Science Publications, Oxford, British, 1994.
[13] James E. Broadwell, Shock structure in a simple discrete velocity gas, The Physics of Fluids 7 (1964) 1243–1247.
[14] Cedric Croizet, Renee Gatignol. Kinetic description for a suspension of inelastic spheres-Boltzmann and BGK equations, in: Rarefied Dynamics: 22nd International Symposium, 2001:859–866.
[15] Yoshio Sone, Taku Ohwada, Kazuo Aoki, Temperature jump and Knudsen layer in a rarefied gas over a plane wall: numerical analysis of the linearized Boltzmann equation for hard-sphere molecules, Physics of Fluids A–Fluid Dynamics 2 (1989) 363–370.
[16] Felix Sharipov, Application of the Cercignani–Lampis scattering kernel to calculations of rarefied gas flows I. Plane flow between two parallel plates, European Journal of Mechanics B/Fluids 21 (2002) 113–123.
[17] Felix Sharipov, Application of the Cercignani–Lampis scattering kernel to calculations of rarefied gas flows. II. Slip and jump coefficients, European Journal of Mechanics B/Fluids 22 (2003) 133–143.
[18] Y. Sone, S. Taka, T. Ohwada, Numerical analysis of the plane Couette flow of a rarefied gas on the basis of the linearized Boltzmann equation for hard-sphere molecules, European Journal of Mechanics B/Fluids 9 (1990) 273–288.
[19] Felix Sharipov, Vladimir Selezner, Data on internal rarefied gas flows, Journal of Physical and Chemical Reference Data 27 (1993) 657–706.
[20] James E. Broadwell, Study of rarefied gas flow by the discrete velocity method, Journal of Fluid Mechanics 19 (1964) 401–414.
[21] Taku Ohwada, Yoshio Sone, Kazuo Aoki, Numerical analysis of the shear and thermal creep flows of a rarefied gas over a plane wall on the basis of the linearized Boltzmann equation for hard-sphere molecules, Physics of Fluids A–Fluid Dynamics 9 (1989) 1588–1599.
[22] Taku Ohwada, Yoshio Sone, Kazuo Aoki, Numerical analysis of the Poiseuille and thermal transpiration flows between two parallel plates on the basis of the Boltzmann equation for hard-sphere molecules, Physics of Fluids A–Fluid Dynamics 12 (1989) 2042–2049.
[23] S. Naris, D. Valougeorgis, F. Sharipov, D. Kalempa, Discrete velocity modeling of gaseous mixture flows in MEMS, Superlattices and Microstructures 35 (2004) 629–643.
[24] A.V. Bobylev, Exact solutions of discrete kinetic models and stationary problems for the plane Broadwell model, Mathematical Methods in the Applied Sciences 19 (1996) 825–845.
[25] Taku Ohwada, Heat flow and temperature and density distributions in a rarefied gas between parallel plates with different temperatures. Finite-difference analysis of the nonlinear Boltzmann equation for hard-sphere molecules, The Physics of Fluids 8 (1996) 2153–2160.

[26] Anerdw J. Christlieb, W. Nicholas, G. Hitchon, Iain D. Boyd, Quanhua Sun, Kinetic description of flow past a micro-plate, Journal of Computational Physics 195 (2004) 508–527.
[27] J. Feng, W.N.G. Hitchon, Boltzmann equation description of flows at long mean free paths, Physical Review E 70 (2004) 1–10.
[28] R. Gatignol, Kinetic theory boundary condition for discrete velocity gases, The Physics of Fluids 20 (1977) 2022–2030.
[29] R. Gatignol, Kinetic theory for a discrete velocity gas and application to the shock structure, The Physics of Fluids 18 (1975) 153–161.
[30] Felix Sharipov, Application of the Cercignani–Lampis scattering kernel to calculations of rarefied gas flows. III. Poiseuille flow and thermal creep through a long tube, European Journal of Mechanics B/Fluids 22 (2003) 145–154.
[31] Hans Babovsky, Diffusion limits for flows in thin layers, SIAM Journal on Applied Mathematics 56 (1996) 1280–1294.
[32] Christoph Borgers, Claude Greengard, Enrique Thomann, The diffusion limit of free molecular flow in thin plane channels, SIAM Journal on Applied Mathematics 52 (1992) 1057–1075.
[33] Christian Dogbe, Anomalous diffusion limit induced on a kinetic equation, Journal of Statistical Physics 100 (2000) 603–632.
[34] Andrew J. Christlieb, James A. Rossmanith, Peter Smereka, The broadwell model in a thin channel, Communications in Mathematical Sciences 2 (2004) 443–476.